

Strain-induced antiferromagnetic domain switching via the spin Jahn-Teller effect

Dylan Behr,^{1,*} Leonid S. Taran,² Daniel G. Porter,³ Alessandro Bombardi,³ Dharmalingam Prabhakaran,⁴ Sergey V. Streltsov,^{2,5} and Roger D. Johnson^{1,3}

¹*Department of Physics and Astronomy, University College London, Gower Street, London WC1E 6BT, United Kingdom*

²*M. N. Mikheev Institute of Metal Physics, Ural Branch of Russian Academy of Sciences, 620137 Yekaterinburg, Russia*

³*Diamond Light Source, Rutherford Appleton Laboratory-STFC, Chilton, Didcot OX11 0QX, United Kingdom*

⁴*Department of Physics, University of Oxford, Clarendon Laboratory, Parks Road, Oxford OX1 3PU, United Kingdom*

⁵*Institute of Physics and Technology, Ural Federal University, 620002 Yekaterinburg, Russia*



(Received 13 November 2023; accepted 29 July 2024; published 15 August 2024)

The spin Jahn-Teller effect, where a degeneracy of magnetic ground states is spontaneously lifted by structural distortions, lends itself to exploitation by the implied magnetoelastic coupling. CoTi_2O_5 hosts a frustrated topology of magnetic interactions that could realize such coupling, since the observed magnetic ground state requires a spontaneous monoclinic distortion of the crystal. Using resonant elastic x-ray scattering to simultaneously probe the magnetic structure and lattice distortion of CoTi_2O_5 , we demonstrate near complete magnetic domain switching by an applied uniaxial stress that is conjugate to the monoclinic strain. Our results, supported by density functional theory calculations, confirm that CoTi_2O_5 displays spin Jahn-Teller effects that can be understood in terms of modulated Heisenberg exchange interactions, and demonstrate the potential functionality of spin Jahn-Teller materials in spintronic devices sensitive to uniaxial strain.

DOI: [10.1103/PhysRevB.110.L060408](https://doi.org/10.1103/PhysRevB.110.L060408)

The interplay between structural and electronic degrees of freedom in crystalline materials gives rise to a rich variety of phase transitions, providing not just a setting to explore fundamental materials physics, but also numerous opportunities for technological exploitation. Such relationships encompass topical phenomena such as magnetoelectric coupling [1,2], and (*pseudo*) Jahn-Teller effects in which a variety of electronic instabilities drive spontaneous crystal distortions [3,4]. In such cases the role of the crystal structure in mediating microscopic interactions provides a powerful lever for manipulating the electronic ground state, and the use of uniaxial stress has emerged as an effective controllable conjugate field. The respective strain may act both as a tuning parameter within a given phase, and as a symmetry-breaking distortion, activating new terms in the Hamiltonian. Eminent examples that demonstrate the effectiveness of stress in tuning material properties include the control of superconductivity and charge-density waves [5–8], antiferromagnetic (AFM) ordering [9,10], metal-insulator transitions [11,12], and bulk ferromagnetism [13].

The ability to switch magnetic domains via applied strain is a highly sought-after capability in the spintronics community, where efforts to realize robust magnetic data storage and manipulation by strain control of magnetic domain walls have achieved numerous successes in

ferromagnetic thin films via ferroelectric and piezoelectric substrates [14–16]. In antiferromagnetic (AFM) systems, for which faster dynamics and robustness against perturbation from magnetic fields can be achieved, studies aimed at domain control have typically focused on Néel vector domains related by rotational symmetries of the paramagnetic parent and stabilized by magnetocrystalline anisotropy [17–20]. An alternative strategy to achieve strain-induced domain switching is to directly modulate the magnetic exchange topology, thereby energetically selecting a given magnetostructural domain. One system with a suitable exchange topology is CoTi_2O_5 , in which a transition from low-dimensional magnetism [21] to long-range antiferromagnetic order occurs at $T_N = 26$ K. The resultant four magnetic domains are associated with two propagation vectors $\mathbf{k}_\pm = (\frac{1}{2}, \pm\frac{1}{2}, 0)$, defined with respect to the orthorhombic parent, and broken time reversal symmetry ($2k$ -vector (magnetostructural) $\times 2$ time-reversal = 4 magnetic domains). Domains of different \mathbf{k} are interrelated by mirror symmetries broken at the transition [21]. Though changes to the crystal structure have not been reported, a concomitant lattice distortion is implied by a phenomenological magnetostructural coupling invariant, which can be aptly understood in the framework of spin Jahn-Teller theory [22–24]. Here, symmetry-lowering monoclinic distortions in CoTi_2O_5 lift the degeneracy of magnetic ground states through a modulation of exchange pathways that select either \mathbf{k}_+ or \mathbf{k}_- . This feature suggests that a uniform strain field, conjugate to the monoclinic spin Jahn-Teller strain, can be used to switch between magnetostructural domains.

In this Letter, we present a combined resonant elastic x-ray scattering (REXS) and density functional theory (DFT) study

*Contact author: dylan.behr.20@ucl.ac.uk

of CoTi_2O_5 . We demonstrate nearly complete antiferromagnetic domain switching in a single crystal by application of uniaxial stress in a direction determined by symmetry analysis of the magnetostructural phase transition. Reversing the causal relationship between magnetism and the lattice, strain selection of \mathbf{k}_\pm domains not only represents an original domain switching mechanism, but also substantiates the physical interpretation of the transition based on the spin Jahn-Teller effect.

Single crystals of CoTi_2O_5 were cut such that their long axis was aligned with the $(1, \bar{1}, 0)$ reciprocal lattice vector, and an elongated top face was normal to the crystallographic c axis and polished to a mirror finish. Further details of the synthesis and preparation of crystals are presented in the Supplemental Material [26] (see also Refs. [27–36] therein). REXS measurements were performed in reflection geometry $[(0, 0, l)$ specular] on the I16 beamline at Diamond Light Source with x rays tuned to the Co K edge. We use σ and π to denote linear polarization perpendicular and parallel to the scattering plane, respectively. Primed and unprimed symbols refer to the scattered and incident beams. For each sample, a number of Bragg reflections were identified and used to determine the exact orientation of the crystal with respect to the diffractometer angles. Lattice parameters of $a = 3.732$, $b = 9.718$, and $c = 10.069$ Å were found at a base temperature of 7 K, consistent with the orthorhombic $Cmcm$ unit cell established by Ref. [21].

The first sample was mounted directly onto a copper plate and cooled to low temperature. New diffraction peaks appeared below T_N at satellite positions $\mathbf{Q}_0 \pm \mathbf{k}_+$ and $\mathbf{Q}_0 \pm \mathbf{k}_-$, originating in scattering from \mathbf{k}_+ and \mathbf{k}_- domains, respectively, where \mathbf{Q}_0 indexes an allowed structural Bragg peak [see Fig. 1(a) for satellites of the Bragg peak at $\mathbf{Q}_0 = (0, 0, 9)$]. The magnetic origin of the new intensities was confirmed by determining their polarization, energy, and temperature dependencies: At 7 K no signal was detectable at $\mathbf{Q}_0 + \mathbf{k}_+$ in the σ - σ' channel, while in σ - π' a strong resonant intensity was recorded [Figs. 1(b)–1(d)], as expected for $E1$ - $E1$ scattering events from parity-even, time-reversal-odd (magnetic) dipoles [37]. The integrated intensity of the magnetic peaks, being proportional to the squared magnitude of magnetic moments on Co^{2+} sites, showed a typical order parameter dependence on temperature [Fig. 1(e)]. Fitting of the temperature dependence gave a critical exponent of $\beta \sim 0.21(5)$ (we note that this value should be taken lightly as the density of measured intensities is low in the critical region), $\alpha \sim 5.2(8)$, and a transition temperature of $T_N = 26$ K, in good agreement with the value determined by bulk studies [21]. The energy dependence on diffraction intensity shows the main K -edge resonance at 7.724 keV appearing exclusively in the σ - π' channel and a large pre-edge feature at 7.709 keV [Fig. 1(f)] recorded in both polarization channels. This pre- K -edge resonance is consistent with $E1$ - $E2$ scattering events from parity-odd, time-reversal-odd multipoles, which are allowed by the lack of inversion centres at Co $4c$ sites (site symmetry $m2m$) [38]. A lower bound on the spatial extent of magnetic correlations can be obtained from the half width of peaks scanned in momentum space, giving minimum correlation lengths of approximately 600, 300, and 800 nm along a , b , and c , respectively. The widths of the magnetic peaks are comparable

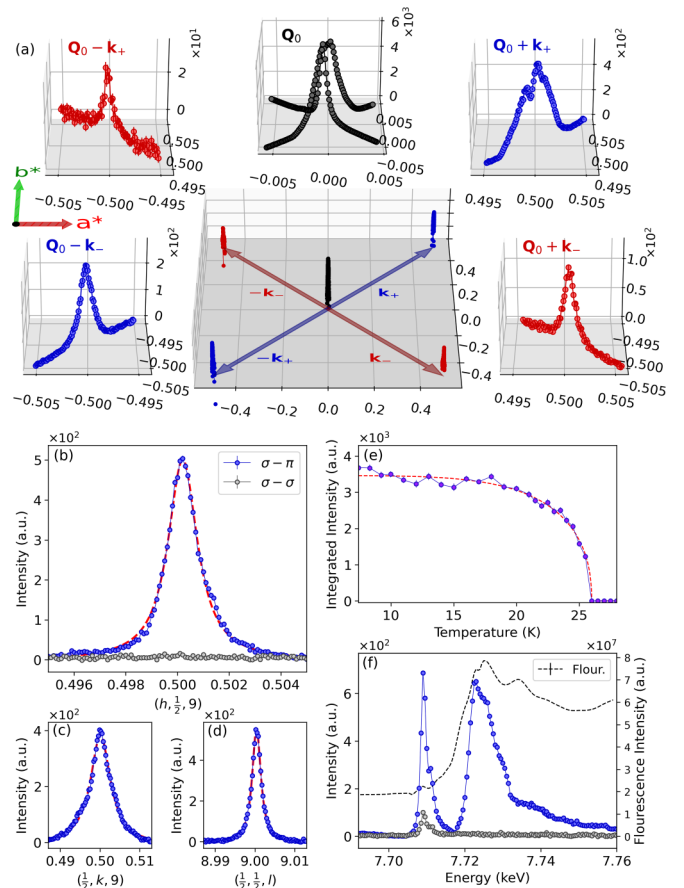


FIG. 1. (a) Structural, $\mathbf{Q}_0 = (0, 0, 9)$, and magnetic, $\mathbf{Q}_0 \pm \mathbf{k}_+$ and $\mathbf{Q}_0 \pm \mathbf{k}_-$, diffraction intensities measured below T_N and at an energy of 7.724 keV, shown in black, blue, and red, respectively (logarithmic intensity scale in the central plot). The peak splitting observed at $\mathbf{Q}_0 + \mathbf{k}_+$ was due to sample mosaicity. (b)–(d) Scans along \mathbf{a}^* , \mathbf{b}^* , and \mathbf{c}^* through the magnetic peak at $\mathbf{Q}_0 + \mathbf{k}_+$. Blue and gray data points show intensities recorded in the σ - π' and σ - σ' polarization channels, respectively. Red dashed lines are pseudo-Voigt fits. (e) Temperature dependence of the integrated intensity of the $\mathbf{Q}_0 + \mathbf{k}_+$ peak, with the red dashed line representing a fit to the functional form $I = I_0[1 - (T/T_N)^\alpha]^{2\beta}$ [25]. (f) Energy scans of the $\mathbf{Q}_0 + \mathbf{k}_+$ intensity in both polarization channels, with fluorescence overlaid as a black dashed line.

to that of the nearby structural Bragg peak \mathbf{Q}_0 , indicating that the magnetic order is well developed and on a comparable range to the structural order. By raster scanning across the sample while measuring the relative intensities of the $\mathbf{Q}_0 + \mathbf{k}_+$ and $\mathbf{Q}_0 + \mathbf{k}_-$ magnetic peaks, we can reconstruct the domain configuration close to the sample surface, as shown in Figs. 2(a)–2(c). The lateral size of magnetostructural domains were observed to be >0.3 mm. We note that, as in Ref. [21], structural Bragg peak splitting resulting from the spontaneous monoclinic distortion at T_N could not be resolved. That no evidence of structural symmetry breaking was observed may not be surprising. For example, in the case of magnetoelectric multiferroics a spin-induced polarization and switchable polar domains can be measured [39,40], while the respective structural distortions occur at the femtoscale and are seldom observed [41].

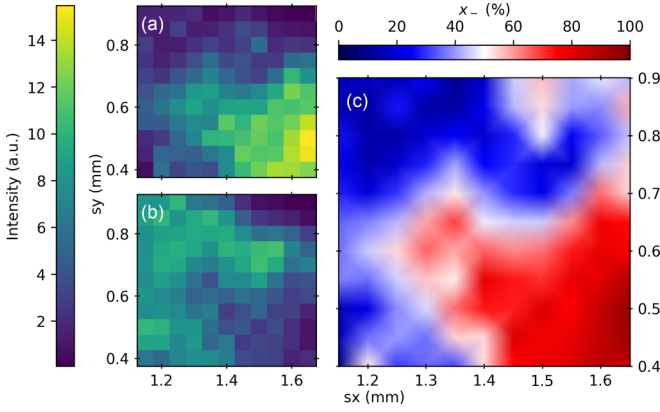


FIG. 2. (a) $\mathbf{Q}_0 + \mathbf{k}_- = (\frac{1}{2}, -\frac{1}{2}, 9)$ and (b) $\mathbf{Q}_0 + \mathbf{k}_+ = (\frac{1}{2}, \frac{1}{2}, 9)$ magnetic intensities raster mapped across the sample surface. (c) \mathbf{k} domain fraction (Gouraud interpolated) calculated using $x_{\pm} = I_{\pm}/(I_+ + I_-)$.

A second crystal was mounted in a Razorbill Instruments CS100 compensated piezoelectric strain cell, with the long axis [parallel to $(1, \bar{1}, 0)$] of the crystal spanning a gap between opposing bridges of the cell, as shown in Fig. S1 of the Supplemental Material [26]. The uniaxial stress applied in this direction results in a shear strain field represented by the infinitesimal strain tensor

$$\begin{bmatrix} 0 & e_{xy} & 0 \\ e_{xy} & 0 & 0 \\ 0 & 0 & 0 \end{bmatrix},$$

which transforms by the Γ_2^+ irrep. With the cell installed inside a standard closed cycle refrigerator (CCR), the distance between the two bridges could be varied by applying a voltage difference across the piezoelectric stacks, leading to a controlled strain, $\Delta L/L \equiv \Delta d_{1\bar{1}0}/d_{1\bar{1}0}$, on the sample.

$\Delta L/L$ was quantified as a function of applied voltage by measuring the 2θ positions of coplanar intensities at $(1, \bar{1}, 4)$ and $(0, 0, 10)$, permitting calculation of the interplanar distance $d_{1\bar{1}0}$ (see Supplemental Material [26]). Hence, the strain was calibrated within exactly the same sample volume (penetrated by the beam) from which magnetic diffraction intensities were measured.

With the temperature held at 7 K, the intensities of the $\mathbf{Q}_0 + \mathbf{k}_+$ and $\mathbf{Q}_0 + \mathbf{k}_-$ peaks were integrated while changing the applied voltage between -80 and 60 V at 5 V intervals such that the induced strain along $(1, \bar{1}, 0)$ transitioned from compressive to tensile. The resulting values were then used to calculate \mathbf{k}_{\pm} domain fractions, which are plotted against strain in Fig. 3(d). Additionally, domain maps were produced from raster scans of the $\mathbf{Q}_0 + \mathbf{k}_+$ and $\mathbf{Q}_0 + \mathbf{k}_-$ peak intensities at -80 and 60 V, corresponding to states of maximal compressive and tensile strain, respectively [Figs. 3(a)–3(c) and 3(e)–3(g)]. The results demonstrate near total switching of magnetostructural domains with strain. Temperature dependencies of the magnetic intensities were also measured at states of maximal strain, evidencing no detectable change in the ordering temperature [see Fig. 3(d) inset].

A comprehensive symmetry analysis presented in Ref. [21] showed that the \mathbf{k}_+ and \mathbf{k}_- magnetic domains of CoTi_2O_5 transform as the mS_2^- irreducible representation (irrep) with $(\eta, 0)$ and $(0, \epsilon)$ order parameter directions, respectively. A phenomenological magnetoelastic free-energy invariant $\delta(\eta^2 - \epsilon^2)$ was proposed to facilitate long-range magnetic ordering via the spin Jahn-Teller effect, based on coupling to a monoclinic displacive mode transforming as the Γ_2^+ irrep with order parameter δ . Here, the sign of δ selects a given single- \mathbf{k} domain, and it follows that by introducing a strain mode that also transforms by Γ_2^+ (note $+\Delta L/L$ corresponds to $-\delta$, and vice versa), one can energetically bias domains transforming as $(\eta, 0)$ or $(0, \epsilon)$. Thus, our experimental results confirm the proposed phenomenological model.

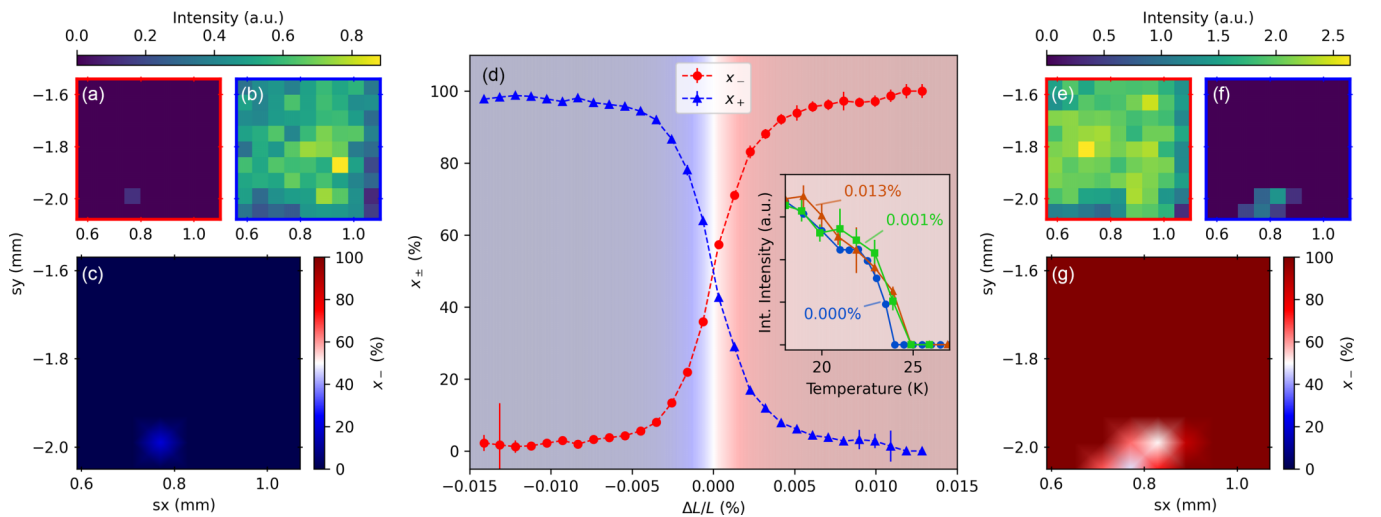


FIG. 3. (a) and (b) depict raster maps of $\mathbf{Q}_0 + \mathbf{k}_-$ and $\mathbf{Q}_0 + \mathbf{k}_+$ intensities, respectively, across a region of the sample surface at a voltage of -80 V (maximal compressive strain). (c) Domain map calculated using $x_{\pm} = I_{\pm}/(I_+ + I_-)$ showing a near single \mathbf{k}_+ domain. (d) depicts the dependence of x_{\pm} domain fractions on strain as determined by the relative intensities of $\mathbf{Q}_0 + \mathbf{k}_-$ and $\mathbf{Q}_0 + \mathbf{k}_+$. The inset shows the temperature dependencies of the $\mathbf{Q}_0 + \mathbf{k}_-$ magnetic intensity at various strains. (e)–(g) were produced in the same manner as (a)–(c) at a voltage of 60 V (maximal tensile strain).

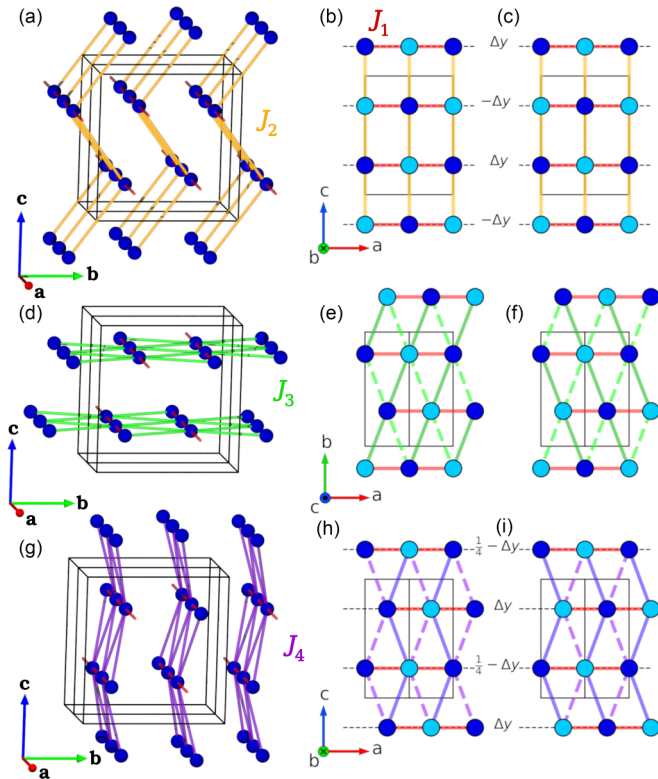


FIG. 4. (a), (d), and (g) depict “sheets” of Co^{2+} ions (blue spheres) defined by exchange pathways J_1 (red) and J_2 (amber), J_1 (red) and J_3 (green), and J_1 (red) and J_4 (purple), respectively. (b), (e), and (h) show projections of single sheets with antiparallel moments colored light and dark blue as in the \mathbf{k}_+ domain. The Γ_2^+ splitting of J_3 (J_4) is depicted as dark solid and light dashed connections. (c), (f), and (i) are corresponding diagrams for the \mathbf{k}_- domain.

Total energy DFT+ U calculations based on the undistorted crystal structure (for details, see Supplemental Material [26]), show that \mathbf{k}_+ and \mathbf{k}_- magnetic domains are degenerate to within 4 mK/f.u. [42]. The Γ_2^+ strain described above will introduce a slight modulation in the exchange parameters, resulting in a very small energy difference between \mathbf{k}_+ and \mathbf{k}_- domains, labeled ΔE . In order to reliably calculate ΔE , the strains were amplified to generate a set of model distorted structures. DFT+ U results shown in Fig. S3 confirm that positive strain ($\Delta L/L > 0$) does indeed stabilize the \mathbf{k}_- domain, and that this effect can be reversed. Furthermore, structural relaxations indicate subtle magnetostrictive distortions in opposite directions for \mathbf{k}_+ and \mathbf{k}_- domains, resulting in a shortening of the corresponding Co-Co bond on the order of $\sim 10^{-4}$ Å. Such distortions are typically too small to be resolved by state-of-the-art diffraction techniques, further corroborating the absence of observable peak splitting in either the present or prior studies on the unstressed system.

The AFM structures of CoTi_2O_5 are stabilized by a network of frustrated exchange interactions, as depicted in Fig. 4. For both domains, buckled sheets of Co^{2+} ions adopt Néel-type antiferromagnetic order on a distorted square lattice spanned by nearest-neighbor superexchange and supersuperexchange interactions labeled J_1 and J_2 , respectively [see Figs. 4(a)–4(c)]. These buckled sheets represent unfrustrated

subunits common to both domains. Connecting each AFM buckled sheet to its neighbor (related by a $[\frac{1}{2}, \frac{1}{2}, 0]$ translation) are interlayer exchanges J_3 and J_4 [see Figs. 4(d)–4(f) and 4(g)–4(i), respectively]. These are also weak supersuperexchange pathways which, in the paramagnetic $Cmcm$ symmetry, perfectly frustrate the magnetic structure. The $m2m$ site symmetry of Co^{2+} ions forbids the presence of a net J_3 or J_4 exchange field at any given site, since equal numbers of antialigned moments from the neighboring AFM sheets contribute with the same coupling strength. The effect is that the AFM J_1 – J_2 sheets are decorrelated from one another. However, Γ_2^+ distortions induced either spontaneously at a spin Jahn-Teller transition, or by application of stress described above, lowers the site symmetry of Co^{2+} ions to m_z , splitting the interlayer exchanges into inequivalent pairs J_3/J_3' and J_4/J_4' . This establishes the sign of the exchange field, and therefore the relative phase between neighboring AFM sheets, giving long-range magnetic order with a \mathbf{k}_+ or \mathbf{k}_- propagation vector. For its part, total energy DFT+ U calculations show that $J_1 \approx 16.8$ K (AFM), in excellent agreement with J determined by fitting magnetic susceptibility [26]. Both J_3 and J_4 were found to be small (~ 0.2 K), and the magnitude of J_2 was below the resolution of the calculations. We suggest that the DFT+ U approach is not accurate enough to estimate the subtle differences in exchange associated with the spin Jahn-Teller distortions. Nonetheless, the perfect frustration of J_3 and J_4 exchanges in orthorhombic symmetry, and therefore the degeneracy of \mathbf{k}_\pm domains, can only be lifted in the presence of Γ_2^+ distortions.

At the mean-field level, the bulk ordering temperature is determined by an aggregate of the exchange interaction energies. Therefore, when strain lifts the magnetic frustration of J_3 and J_4 , one might expect a significant increase in T_N . It was surprising, therefore, that no such increase was observed in the stressed samples. Thermodynamically, the stress dependence of the critical temperature is captured by the modified Ehrenfest relation for second-order phase transitions [43,44],

$$\frac{dT_N}{d\sigma} = \frac{\Delta\alpha_\delta T_0}{\Delta C_\sigma}, \quad (1)$$

where σ is the stress component coupling to the strain, T_0 is the transition temperature in zero applied stress, and ΔC_σ and $\Delta\alpha_\delta$ are discontinuities in the heat capacity and thermal distortion coefficient $\alpha_\delta \equiv (\frac{\partial\delta}{\partial T})$ across the transition, respectively. The above relation is derived from a Landau theory in the Supplemental Material [26]. Diffraction experiments have shown no detectable change in crystal structure at T_N [21], suggesting a very small value of $\Delta\alpha_\delta$. Hence, the stress dependence of the transition temperature is likely very weak, explaining the insensitivity of T_N to strain. Despite this, remarkably small strains are sufficient to stabilize \mathbf{k} domains.

In summary, we have demonstrated an approach to control AFM domains by applied stress through exploiting the spin Jahn-Teller effect in CoTi_2O_5 —a material system that offers numerous opportunities to the wider frustrated magnetism community for its complex frustrated exchange topology, and for the involvement of Co^{2+} ions that host large spin-orbit coupling. Looking beyond CoTi_2O_5 , AFM domain switching is typically achieved by tuning magnetocrystalline anisotropies [45]. Instead, we have shown that

spin Jahn-Teller-based magnetoelastic coupling, which modulates magnetic frustration arising from competing Heisenberg exchange pathways, can enable direct control of different k domains. This mechanism may be generalized to account for the properties of other material systems. For example, previous studies on CeAl_2 demonstrating multi- k -domain switching by uniaxial strain [46,47] can now be understood in the context of spin Jahn-Teller theory [23]. Furthermore, progress towards room-temperature spin Jahn-Teller phase transitions could lead to striking developments in the field of spintronics. If such a material can be incorporated into a suitable thin-film heterostructure with a piezoelectric substrate,

antiferromagnetic domain structures could be deterministically manipulated by an electric field.

We thank Diamond Light Source for access to beamline I16 (MM32034) that contributed to the results presented here. R.D.J. acknowledges support from a Diamond Light Source Collaboration Agreement, while S.V.S. thanks Russian Science Foundation (RSF 23-12-00159; strain calculations) and L.S.T. “Quantum” project (122021000038-7; exchange calculations). D.P. acknowledges the Engineering and Physical Sciences Research Council (EPSRC), U.K., and the Oxford-ShanghaiTech collaboration project for financial support.

-
- [1] S.-W. Cheong and M. Mostovoy, Multiferroics: A magnetic twist for ferroelectricity, *Nat. Mater.* **6**, 13 (2007).
- [2] D. Khomskii, Classifying multiferroics: Mechanisms and effects, *Physics* **2**, 20 (2009).
- [3] D. I. Khomskii, *Transition Metal Compounds* (Cambridge University Press, Cambridge, UK, 2014).
- [4] A. Ceulemans, *The Theory of the Jahn-Teller Effect: When a Boson Meets a Fermion* (Springer, Berlin, 2022).
- [5] A. Steppke, L. Zhao, M. E. Barber, T. Scaffidi, F. Jerzembeck, H. Rosner, A. S. Gibbs, Y. Maeno, S. H. Simon, A. P. Mackenzie, and C. W. Hicks, Strong peak in T_c of Sr_2RuO_4 under uniaxial pressure, *Science* **355**, eaaf9398 (2017).
- [6] H. H. Kim, S. M. Souliou, M. E. Barber, E. Lefrançois, M. Minola, M. Tortora, R. Heid, N. Nandi, R. A. Borzi, G. Garbarino, A. Bosak, J. Porras, T. Loew, M. König, P. M. Moll, A. P. Mackenzie, B. Keimer, C. W. Hicks, and M. Le Tacon, Uniaxial pressure control of competing orders in a high-temperature superconductor, *Science* **362**, 1040 (2018).
- [7] H.-H. Kim, E. Lefrançois, K. Kummer, R. Fumagalli, N. B. Brookes, D. Betto, S. Nakata, M. Tortora, J. Porras, T. Loew, M. E. Barber, L. Braicovich, A. P. Mackenzie, C. W. Hicks, B. Keimer, M. Minola, and M. Le Tacon, Charge density waves in $\text{YBa}_2\text{Cu}_3\text{O}_{6.67}$ probed by resonant x-ray scattering under uniaxial compression, *Phys. Rev. Lett.* **126**, 037002 (2021).
- [8] P. Malinowski, Q. Jiang, J. J. Sanchez, J. Mutch, Z. Liu, P. Went, J. Liu, P. J. Ryan, J. W. Kim, and J. H. Chu, Suppression of superconductivity by anisotropic strain near a nematic quantum critical point, *Nat. Phys.* **16**, 1189 (2020).
- [9] C. Dhital, Z. Yamani, W. Tian, J. Zeretsky, A. S. Sefat, Z. Wang, R. J. Birgeneau, and S. D. Wilson, Effect of uniaxial strain on the structural and magnetic phase transitions in BaFe_2As_2 , *Phys. Rev. Lett.* **108**, 087001 (2012).
- [10] T. Janssen, M. Gidding, C. S. Davies, A. V. Kimmel, and A. Kirilyuk, Strain-induced magnetic pattern formation in antiferromagnetic iron borate, *Phys. Rev. B* **108**, L140405 (2023).
- [11] N. B. Aetukuri, A. X. Gray, M. Drouard, M. Cossale, L. Gao, A. H. Reid, R. Kukreja, H. Ohldag, C. A. Jenkins, E. Arenholz, K. P. Roche, H. A. Dürr, M. G. Samant, and S. S. Parkin, Control of the metal-insulator transition in vanadium dioxide by modifying orbital occupancy, *Nat. Phys.* **9**, 661 (2013).
- [12] S. Riccò, M. Kim, A. Tamai, S. McKeown Walker, F. Y. Bruno, I. Cucchi, E. Cappelli, C. Besnard, T. K. Kim, P. Dudin, M. Hoesch, M. J. Gutmann, A. Georges, R. S. Perry, and F. Bamberger, *In situ* strain tuning of the metal-insulator transition of Ca_2RuO_4 in angle-resolved photoemission experiments, *Nat. Commun.* **9**, 4535 (2018).
- [13] A. Najev, S. Hameed, D. Gautreau, Z. Wang, J. Joe, M. Požek, T. Birol, R. M. Fernandes, M. Greven, and D. Pelc, Uniaxial strain control of bulk ferromagnetism in rare-earth titanates, *Phys. Rev. Lett.* **128**, 167201 (2022).
- [14] O. Rousseau, R. Weil, S. Rohart, and A. Mougin, Strain-induced magnetic domain wall control by voltage in hybrid piezoelectric BaTiO_3 ferrimagnetic TbFe structures, *Sci. Rep.* **6**, 23038 (2016).
- [15] R. G. Hunt, K. J. A. Franke, P. M. Shepley, and T. A. Moore, Strain-coupled domains in $\text{BaTiO}_3(111)$ -CoFeB heterostructures, *Phys. Rev. B* **107**, 014409 (2023).
- [16] M. Schmitz, A. Weber, O. Petravic, M. Waschk, P. Zakalek, S. Mattauch, A. Koutsoubas, and T. Brückel, Strain and electric field control of magnetism in $\text{La}_{(1-x)}\text{Sr}_x\text{MnO}_3$ thin films on ferroelectric BaTiO_3 substrates, *New J. Phys.* **22**, 053018 (2020).
- [17] E. A. Tereshina-Chitrova, L. V. Pourovskii, S. Khmelevskiy, L. Horak, Z. Bao, A. Mackova, P. Malinsky, T. Gouder, and R. Caciuffo, Strain-driven switching between antiferromagnetic states in frustrated antiferromagnet UO_2 probed by exchange bias effect, *Adv. Funct. Mater.* **34**, 2311895 (2023).
- [18] Z. Ni, A. V. Haglund, H. Wang, B. Xu, C. Bernhard, D. G. Mandrus, X. Qian, E. J. Mele, C. L. Kane, and L. Wu, Imaging the Néel vector switching in the monolayer antiferromagnet MnPS_3 with strain-controlled Ising order, *Nat. Nanotechnol.* **16**, 782 (2021).
- [19] A. A. Sapozhnik, R. Abrudan, Y. Skourski, M. Jourdan, H. Zabel, M. Kläui, and H. J. Elmers, Manipulation of antiferromagnetic domain distribution in Mn_2Au by ultrahigh magnetic fields and by strain, *Phys. Status Solidi RRL* **11**, 1600438 (2017).
- [20] C. Schmitt, L. Baldrati, L. Sanchez-Tejerina, F. Schreiber, A. Ross, M. Filianina, S. Ding, F. Fuhrmann, R. Ramos, F. Maccherozzi, D. Backes, M. A. Mawass, F. Kronast, S. Valencia, E. Saitoh, G. Finocchio, and M. Kläui, Identification of Néel vector orientation in antiferromagnetic domains switched by currents in NiO/Pt thin films, *Phys. Rev. Appl.* **15**, 034047 (2021).
- [21] F. K. K. Kirschner, R. D. Johnson, F. Lang, D. D. Khalyavin, P. Manuel, T. Lancaster, D. Prabhakaran, and S. J. Blundell, Spin Jahn-Teller antiferromagnetism in CoTi_2O_5 , *Phys. Rev. B* **99**, 064403 (2019).

- [22] Y. Yamashita and K. Ueda, Spin-driven Jahn-Teller distortion in a pyrochlore system, *Phys. Rev. Lett.* **85**, 4960 (2000).
- [23] O. Tchernyshyov, R. Moessner, and S. L. Sondhi, Order by distortion and string modes in pyrochlore antiferromagnets, *Phys. Rev. Lett.* **88**, 067203 (2002).
- [24] O. Tchernyshyov and G. W. Chern, in *Introduction to Frustrated Magnetism: Materials, Experiments, Theory*, Springer Series in Solid-State Sciences, edited by C. Lacroix, P. Mendels, and F. Mila (Springer, Berlin, 2010), Vol. 164, Chap. 11, pp. 269–290.
- [25] R. F. L. Evans, U. Atxitia, and R. W. Chantrell, Quantitative simulation of temperature-dependent magnetization dynamics and equilibrium properties of elemental ferromagnets, *Phys. Rev. B* **91**, 144425 (2015).
- [26] See Supplemental Material at <http://link.aps.org/supplemental/10.1103/PhysRevB.110.L060408> for a description of the sample mounting within the strain cell, calibration of the strain, details of the density functional theory calculations, analysis of magnetic susceptibility data, and the derivation of the Ehrenfest relation.
- [27] B. J. Campbell, H. T. Stokes, D. E. Tanner, and D. M. Hatch, *ISODISPLACE*: A web-based tool for exploring structural distortions, *J. Appl. Crystallogr.* **39**, 607 (2006).
- [28] V. I. Anisimov, F. Aryasetiawan, and A. I. Lichtenstein, First-principles calculations of the electronic structure and spectra of strongly correlated systems: the LDA + U method, *J. Phys.: Condens. Matter* **9**, 767 (1997).
- [29] J. P. Perdew, K. Burke, and M. Ernzerhof, Generalized gradient approximation made simple, *Phys. Rev. Lett.* **77**, 3865 (1996).
- [30] G. Kresse and J. Furthmüller, Efficient iterative schemes for *ab initio* total-energy calculations using a plane-wave basis set, *Phys. Rev. B* **54**, 11169 (1996).
- [31] H. J. Monkhorst and J. D. Pack, Special points for Brillouin-zone integrations, *Phys. Rev. B* **13**, 5188 (1976).
- [32] S. L. Dudarev, G. A. Botton, S. Y. Savrasov, C. J. Humphreys, and A. P. Sutton, Electron-energy-loss spectra and the structural stability of nickel oxide: An LSDA + U study, *Phys. Rev. B* **57**, 1505 (1998).
- [33] P. A. Maksimov, A. V. Ushakov, Z. V. Pchelkina, Y. Li, S. M. Winter, and S. V. Streltsov, *Ab initio* guided minimal model for the “Kitaev” material $\text{BaCo}_2(\text{AsO}_4)_2$: Importance of direct hopping, third-neighbor exchange, and quantum fluctuations, *Phys. Rev. B* **106**, 165131 (2022).
- [34] S. V. Streltsov, A. S. Mylnikova, A. O. Shorikov, Z. V. Pchelkina, D. I. Khomskii, and V. I. Anisimov, Crystal-field splitting for low symmetry systems in *ab initio* calculations, *Phys. Rev. B* **71**, 245114 (2005).
- [35] R. Dingle, M. E. Lines, and S. L. Holt, Linear-chain antiferromagnetism in $[(\text{CH}_3)_4\text{N}][\text{MnCl}_3]$, *Phys. Rev.* **187**, 643 (1969).
- [36] G. R. Wagner and S. A. Friedberg, Linear chain antiferromagnetism in $\text{Mn}(\text{HCOO})_2 \cdot 2\text{H}_2\text{O}$, *Phys. Lett.* **9**, 11 (1964).
- [37] D. Mannix, D. F. McMorrow, R. A. Ewings, A. T. Boothroyd, D. Prabhakaran, Y. Joly, B. Janousova, C. Mazzoli, L. Paolasini, and S. B. Wilkins, X-ray scattering study of the order parameters in multiferroic TbMnO_3 , *Phys. Rev. B* **76**, 184420 (2007).
- [38] V. Scagnoli and S. W. Lovesey, Analysis of azimuthal-angle scans in resonant x-ray Bragg diffraction and parity even and odd atomic multipoles in the multiferroic modification of the terbium manganate TbMnO_3 , *Phys. Rev. B* **79**, 035111 (2009).
- [39] Y. Yamasaki, S. Miyasaka, Y. Kaneko, J. P. He, T. Arima, and Y. Tokura, Magnetic reversal of the ferroelectric polarization in a multiferroic spinel oxide, *Phys. Rev. Lett.* **96**, 207204 (2006).
- [40] M. Kenzelmann, A. B. Harris, S. Jonas, C. Broholm, J. Schefer, S. B. Kim, C. L. Zhang, S. W. Cheong, O. P. Vajk, and J. W. Lynn, Magnetic inversion symmetry breaking and ferroelectricity in TbMnO_3 , *Phys. Rev. Lett.* **95**, 087206 (2005).
- [41] H. C. Walker, F. Fabrizi, L. Paolasini, F. De Bergevin, J. Herrero-Martin, A. T. Boothroyd, D. Prabhakaran, and D. F. McMorrow, Femtoscale magnetically induced lattice distortions in multiferroic TbMnO_3 , *Science* **333**, 1273 (2011).
- [42] We note that exchange interactions in real materials can be complicated, and generally include not only coupling with further neighbors, but also nonbilinear terms. However, DFT calculations take into account all these contributions.
- [43] P. B. Moin, Second-order phase transitions and Ehrenfest equation for strained solids, *Philos. Mag.* **93**, 4593 (2013).
- [44] M. Matsumoto and M. Sigríst, Ehrenfest relations and magnetoelastic effects in field-induced ordered phases, *J. Phys. Soc. Jpn.* **74**, 2310 (2005).
- [45] X. Chen, X. Zhou, R. Cheng, C. Song, J. Zhang, Y. Wu, Y. Ba, H. Li, Y. Sun, Y. You, Y. Zhao, and F. Pan, Electric field control of Néel spin-orbit torque in an antiferromagnet, *Nat. Mater.* **18**, 931 (2019).
- [46] B. Barbara, M. F. Rossignol, J. X. Boucherle, and C. Vettier, Multiple- \vec{q} structure or coexistence of different magnetic phases in CeAl_2 ? *Phys. Rev. Lett.* **45**, 938 (1980).
- [47] A. B. Harris and J. Schweizer, Theoretical analysis of the double-q magnetic structure of CeAl_2 , *Phys. Rev. B* **74**, 134411 (2006).